

1 **An integrated dataset of ground hydrothermal regimes and soil**
2 **nutrients monitored during 2016-2022 in some previously burned**
3 **areas in hemiboreal forests in Northeast China**

4 Xiaoying Li ¹, Huijun Jin ^{1,2,3 *}, Qi Feng ⁴, Qingbai Wu ¹, Hongwei Wang ^{1,2}, Ruixia He ¹,
5 Dongliang Luo ¹, Xiaoli Chang ^{1,5}, Raul-David Şerban ⁶, and Tao Zhan ³

6 ¹ Key Laboratory of Cryospheric Science and Frozen Soil Engineering, Northwest Institute of Eco-Environment
7 and Resources, Chinese Academy of Sciences, Lanzhou 730000, China;

8 ² School of Civil Engineering and Transportation, China-Russia Joint Laboratory of Cold Regions Engineering and
9 Environment, and Permafrost Institute, Northeast Forestry University, Harbin 150040, China;

10 ³ Ministry of Natural Resources Field Observation and Research Station of Permafrost and Cold Regions
11 Environment in the Da Xing'anling Mountains at Mo'he, Natural Resources Survey Institute of Heilongjiang
12 Province, Harbin 150036, China;

13 ⁴ Key Laboratory of Ecohydrology of Inland River Basin, Northwest Institute of Eco-Environment and Resources,
14 Chinese Academy of Sciences, Lanzhou 730000, China;

15 ⁵ Hunan University of Science and Technology, Xiangtan, Hunan 411202, China and;

16 ⁶ Faculty of Agricultural, Environmental and Food Sciences, Free University of Bozen-Bolzano, Bolzano 39100,
17 Italy

18 * Corresponding authors: Huijun Jin (hjjin@nefu.edu.cn) at the School of Civil Engineering and Transportation,
19 Northeast Forestry University, Harbin 150040, China

20 **Abstract:**

21 Under a warming climate, occurrences of wildfires have been increasingly more
22 frequent in boreal and arctic forests during the last few decades. Wildfires can cause
23 radical changes in the forest ecosystems and permafrost environment, such as
24 irreversible degradation of permafrost, succession of boreal forests, rapid and massive
25 losses of soil carbon stock, and increased periglacial geohazards. Since 2016, we have

26 gradually and more systematically established a network for studying soil nutrients and
27 monitoring the hydrothermal state of the active layer and near-surface permafrost in the
28 northern Da Xing'anling (Hinggan) Mountains in Northeast China. The dataset of soil
29 moisture content (0-9.4 m in depth), soil organic carbon (0-3.6 m), total nitrogen (0-3.6
30 m), and total phosphorus and potassium (0-3.6 m) have been obtained by field sampling
31 and ensuing laboratory tests in 2016. The datasets (2017-2022) of ground temperatures
32 (0-20 m) and active layer thickness have been observed by thermistor cables
33 permanently installed in boreholes. The present data can be used to simulate changes
34 in permafrost features under a changing climate and wildfire disturbances and to
35 explore the changing interactive mechanisms of the fire-permafrost-carbon system in
36 the hemiboreal forest. Furthermore, they can provide baseline data for studies and
37 action plans to support the carbon neutralization initiative and assessment of ecological
38 safety and management of the permafrost environment. These datasets can be easily
39 accessed from the National Tibetan Plateau/Third Pole Environment Data Center
40 (<https://doi.org/10.11888/Cryos.tpdc.300933>, Li and Jin, 2024).

41 **1 Introduction**

42 As a key component of the Northern Hemisphere, permafrost and its changes can
43 have substantial consequences for natural and man-made systems (Smith et al., 2022).
44 Moreover, due to its high sensitivity to climate warming, surface disturbances, and
45 human activities, permafrost has undergone extensive degradation during the last six
46 decades (e.g., Biskaborn et al., 2019; Chang et al., 2024; Jin et al., 2000, 2007, 2021,
47 2022, 2023; Li et al., 2022a; Petrov et al., 2022). As one of the most common natural
48 agents and disturbance factors in boreal forests, wildfires can initiate ecosystem
49 renewal at different spatiotemporal scales (Johnstone et al., 2004; Li et al., 2019).
50 Wildfires impact the permafrost environment first by modifying or altering the ground
51 hydrothermal regimes (Jorgenson et al., 2013; Li et al., 2022b; Yoshikawa et al., 2003),
52 and subsequently by inducing modifications or radical/irreversible changes in
53 biogeochemical processes (e.g., Fultz et al., 2016; Li et al., 2023; Ping et al., 2010; Xu

54 et al., 2024). In boreal forests, wildfires have become increasingly more frequent in
55 recent decades under a warming climate and increasing human activities (Boyd et al.,
56 2023; Chen et al., 2023; Knorr et al., 2016; Westerling et al., 2006). Moreover, the
57 region immediately south of the Arctic circle (50°N-67°N) experienced a greater
58 number of vegetation fires compared to the Arctic (north of 67°N) in 2001-2020 (Chen
59 et al., 2023). Although the total burned area on Earth may be declining, the fire behavior
60 is worsening in several regions in 2003–2023, particularly the boreal and temperate
61 conifer biome (Cunningham et al., 2024).

62 In boreal regions, vegetation and soil organic layer are essential buffering and
63 protective layers of the underlying permafrost. The combustion of all vegetation cover
64 and partial or complete removal of the insulating organic layer have direct hydrothermal
65 impacts on permafrost. It reduces the land surface albedo, increases ground surface and
66 cryosol/ice exposure to direct solar radiation, and weakens the effects of vegetative
67 shading and evapotranspirative cooling (Johnstone et al., 2010; Nossov et al., 2013;
68 Shur and Jorgenson, 2007; Yoshikawa et al., 2003). All of these contribute to higher
69 ground surface temperature and more heat transferred into the ground, resulting in a
70 rapid ground warming and sharp deepening of the active layer (Li et al., 2022b;
71 Michaelides et al., 2019; Nossov et al., 2013; Smith et al., 2015). In the boreal zone, 6-
72 11 years after fire, mean annual ground temperature (MAGT) increased by 1.5-2.3°C
73 (Li et al., 2021; Munkhjargal et al., 2020; Nossov et al., 2013; Smith et al., 2015), even
74 mean annual ground surface temperatures in burned areas were still 2-3°C higher than
75 that in unburned areas 80 years after fire (Brown et al., 2015). Meanwhile, 25 years
76 after fire, the active layer thickness (ALT) could increase by 2.75 m, and ALT could not
77 recover to the pre-fire level even 36 years after fire (Viereck et al., 2008). In Central
78 Siberia, it generally takes 70-80 years for the active layer to return to the pre-fire state
79 (Kirdyanov et al., 2020). In addition, forest fires result in decrease in soil moisture
80 content, which in turn affects ground thermal regimes (Nossov et al., 2013). Moreover,
81 changes in ground hydrothermal regimes and ALT would decline and progressively
82 dwindle with ecosystem recovery and organic layer regrowth over time under a stable

83 or cooling climate (e.g. Holloway et al., 2020; Rocha et al., 2012).

84 Wildfire disturbances also have important and long-term ramifications for
85 terrestrial carbon cycling and carbon stocks (Chen et al., 2022; Dieleman et al., 2022;
86 Genet et al., 2013; O'Donnell et al., 2011a, 2011b). Unlike gradual thawing, abrupt
87 changes after fires in ground hydrothermal regimes often disrupt the entire soil profile
88 and initiate or aggravate carbon loss from deep permafrost soils (Jones et al., 2015;
89 Turetsky et al., 2019). Therefore, the combustion of vegetation and the subsequent thaw
90 of permafrost have resulted in rapid releases of large amounts of carbon and nitrogen
91 into the atmosphere as greenhouse gases (Mack et al., 2011, 2021; Taş et al., 2014).
92 Furthermore, over a short time, abrupt permafrost thaw would possibly result in
93 emitting more methane than gradual thaw (Koven et al., 2015). In addition to soil
94 organic carbon, forest fires potentially also reduce soil nitrogen and phosphorus stocks,
95 inducing shifts in nutrient cycling (Certini, 2005; Gu et al., 2010; Knicker, 2007). For
96 example, one year after wildfire in interior Alaska in the boreal zone, soil carbon
97 content was about 1071-1420 g/m² less at the sites of burned soils than that of unburned
98 soils, and; burned soils had lower nitrogen than unburned soils, higher calcium, and
99 nearly unchanged stocks of potassium, magnesium, and phosphorus (Neff et al., 2005).
100 As a result, wildfires in boreal forest had been considered to trigger strong positive
101 feedbacks on climate warming *via* massive emissions of biogenic major greenhouse gas
102 (Koven et al., 2015; Ramm et al., 2023).

103 Located on the southern margin of Eastern Asian hemiboreal forests and
104 permafrost zones, the Da Xing'anling (Hinggan) Mountains in Northeast China are
105 prone to frequent and massive wildfires. The Xing'an permafrost here is controlled or
106 strongly affected by many local factors, such as dense vegetation cover, thick organic
107 layer, stable snow cover, and anthropic development (Jin et al., 2007; Şerban et al.,
108 2021; Wang et al., 2024). The warm and thin permafrost in the Da Xing'anling
109 Mountains in Northeast China is located in the discontinuous permafrost zone.
110 Therefore, this ecosystem-dominated (driven, modified, or protected) permafrost is
111 sensitive to climate warming and wildfires (Shur and Jorgenson, 2007). Compared with

112 the Arctic permafrost region, the permafrost monitoring network in this region has been
113 established only recently, with inadequately readily accessible and shared permafrost
114 data. Similarly, the permafrost monitoring data in the burned areas in the boreal
115 permafrost region in China are meagre in comparison with those other northern
116 countries or regions, but they are increasing. Prior to the early 1980s, there was little
117 research on wildfire impacts on the permafrost environment in Northeast China. There
118 were only a few occasional fire-related geocryological studies in the early 1990s and
119 limited site-specific measurements of soil temperature and moisture content in the
120 active layer and near-surface (≤ 20 m in depth) permafrost near the Amu'er town,
121 northern Heilongjiang Province (Liang et al., 1991; Zhou et al., 1993). Moreover,
122 research on fire impacts on soil carbon and nitrogen pools and cycles in the Xing'an
123 permafrost in Northeast China has just started and is still at its fledgling stage. Due to
124 the cold and arid climate in winter and spring, complex mountain topography, and dense
125 hemiboreal vegetation in the region, fire regimes are often complex. In addition, burned
126 areas are often located in pristine forest areas far away from roads, making it
127 challenging to timely and/or readily access and study fire impacts. Therefore, it is
128 difficult to systematically understand and quantitatively evaluate the effects of wildfires
129 on ground hydrothermal regimes and carbon stocks at different spatiotemporal scales
130 (Li et al., 2021).

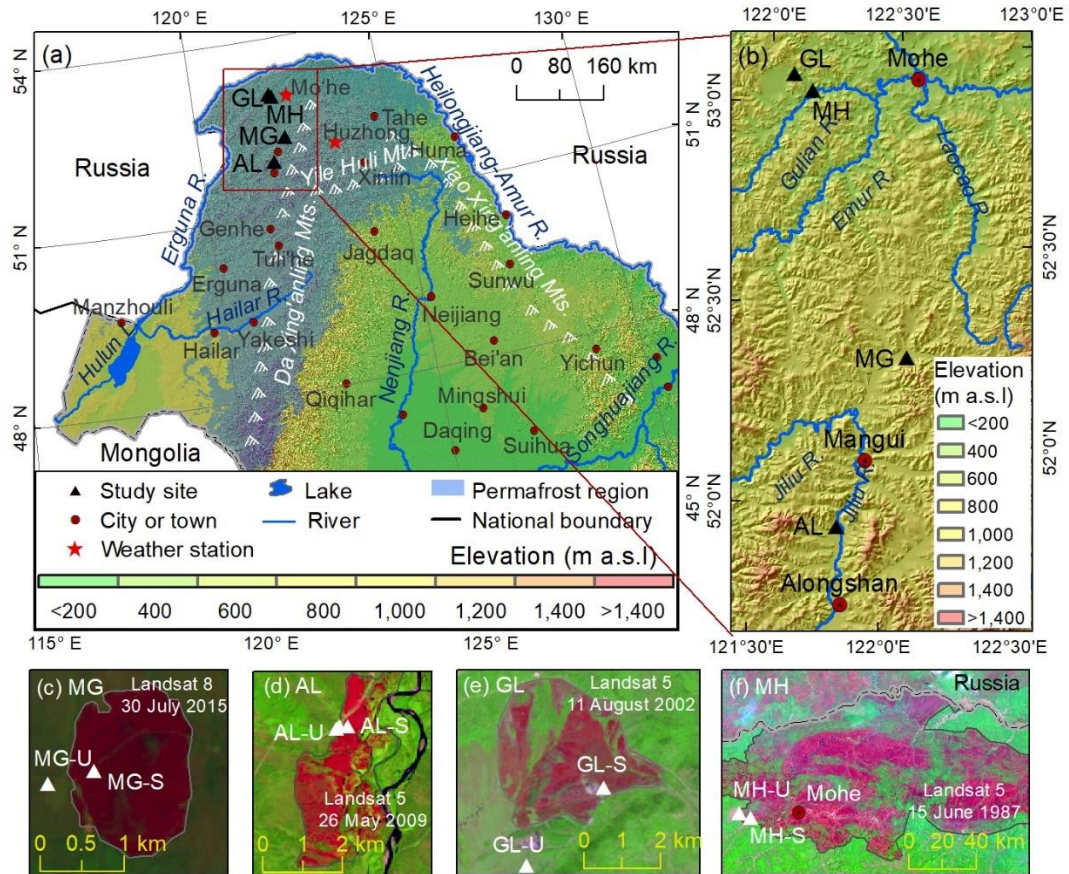
131 To address the abovementioned issues, since 2016, an observation system has been
132 gradually established for ground hydrothermal regimes and soil nutrient contents in the
133 northern Da Xing'anling Mountains. This dataset can provide important supportive data
134 for studying permafrost landscapes, carbon stocks, and boreal ecology and hydrology.
135 It can also provide important references for the management of land and water resources
136 and ecological environment after wildfire disturbances in Northeast China, particularly
137 in forested hemiboreal permafrost regions. In Section 2 of this paper, we first introduce
138 the comprehensive observation network of permafrost and soil nutrients in the northern
139 Da Xing'anling Mountains. The design of the monitoring network of ground
140 hydrothermal regimes and systematic observations of soil nutrient contents, and

141 evaluation of data quality are given in Section 2. In Section 3, observations of
142 permafrost hydrothermal regimes and soil nutrients that provide a 6-year-long dataset
143 are described and briefly interpreted with a focus on major features of the observation
144 network for better understanding of the dataset structure and contents. The data
145 availability and accessibility are provided in Section 4, and; in Section 5, major
146 conclusions and prospects. This dataset provides important input for the model
147 simulations of permafrost changes under fire disturbances and a warming climate,
148 especially those rapid and abrupt degradation of the Xing'an permafrost and resultant
149 periglacial phenomena, such as thermokarst, thaw settlement, and ground surface
150 subsidence and ponding. It is useful for analyzing the interactive hydrothermal and
151 cyclic mechanisms of the wildfires-permafrost-carbon system in the hemiboreal forest.

152 **2 Monitoring networks and data processing**

153 **2.1 Study area descriptions and monitoring networks**

154 A permafrost monitoring network has been established in four burned areas in the
155 northern Da Xing'anling Mountains in Northeast China (Figure 1). Two are located in
156 shrub wetlands in Mo'he city (MH) and Gulian town (GL) in northern Heilongjiang
157 Province. The other two are located in larch forests in Alongshan (AL) and Mangui
158 (MG) towns in the northeastern part of Inner Mongolia. The network includes eight
159 sites in the four burned areas with two fire severity (severely burned (S) and unburned
160 (U)) from 1987 to 2015 (the fire severity division method was shown in "2.2 *Fire*
161 *severity*" section). The studied forest fire in MH (with severely burned (MH-S) and
162 unburned (MH-U) sites) occurred on 6 May 1987, with a burned-over area of 1.01×10^6
163 ha; that in GL (with severely burned (GL-S)) and unburned (GL-U) sites), on 28 July
164 2002, 1,121 ha; AL (with severely burned (AL-S) and unburned (AL-U) sites), on 10
165 May 2009, 930 ha, and; MG (with severely burned (MG-S) and unburned (MG-U) sites),
166 on 12 July 2015, 237 ha.



167

168 Figure 1. Location of the study areas and sites in the northern Da Xing'anling Mountains, Northeast
 169 China.

170 Notes: The base map of permafrost distribution is modified from Li et al. (2022c). The light blue
 171 areas in Figure 1a is the permafrost region. Figures 1c to 1f are the false-color composite image of
 172 the remote sensing image; the burned areas are marked as pink, and the unburned areas are marked
 173 as green.

174 The study areas are characterized by a cold temperate continental climate. In the
 175 study areas of GL and MH, based on the data of nearby Mo'he weather station from
 176 1960 to 2020, mean annual air temperature (MAAT) ranged from -6.2 to -2.4°C , with
 177 an average rate of climate warming at 0.3°C per decade; annual precipitation was 274-
 178 675 mm, with a slight average wetting trend of 13.8 mm per decade. In the study areas
 179 of MG and AL, based on the data of nearby Huzhong weather station from 1974 to 2020,
 180 MAAT varied from -5.2 to -2.0°C , with the same climate warming rate as that of
 181 Mo'he ($0.3^{\circ}\text{C}/\text{decade}$); annual precipitation was 272-749 mm, showing an appreciable
 182 average wetting rate of 3.1 mm per decade. Precipitation fell concentratively in the form

183 of rain from June to August, accounting for 62%-65% of the annual total. Snow cover
 184 generally lasted from October to the next May, with maximum snow depths at 40-50
 185 cm.

186 The four study areas were selected to observe post-fire changes in permafrost
 187 features and soil nutrient conditions (Table 1). This monitoring network includes eight
 188 boreholes and soil profiles, and major elements of the observational network for ground
 189 temperature, ALT, soil moisture content (SMC), soil organic carbon (SOC), total
 190 nitrogen (TN), total phosphorus (TP), and total potassium (TK). The MAGT at the
 191 depth of zero annual amplitude (D_{ZAA} , generally at 10-15 m in depth) ranged from -3.25
 192 to -0.56°C , and measured ALT varied from 1.0 to 3.75 m. The four study areas were
 193 all found in the zones of discontinuous permafrost, with poor drainage in lowlands and
 194 intermontane basins or valleys. Before fires, vegetation was dominated by the Xing'an
 195 larch (*Larix gmelinii*) forest, generally with an understory mainly consisting of the
 196 shrubs *Ledum palustre* and *Vaccinium uliginosum*, with an organic layer of 55-60 cm
 197 in thickness. After fires, the vegetation of burned over areas became gradually
 198 dominated by white birch (*Betula platyphylla*) and dwarf bog birch (*Betula fruticosa*
 199 Pallas), with an organic layer of 20-45 cm in thickness. The soils in the study area are
 200 mainly Histosol and Gelisols (Soil Survey Staff, 2014).

201 Table 1. Characteristics of the eight study sites for monitoring the thermal state and soil nutrients
 202 of the active layer and near-surface permafrost in the northern Da Xing'anling Mountains in

203 Northeast China

Study areas and sites		Lat (°N)	Long. (°E)	Elev. (m a. s. l.)	Veget- -ation	Organic layer thickness (cm)	Drainage	Fire severity
MG (Mangui)	MG-S	52.27 65	122.28 91	710	Larch forest	20	Somewhat poor	Severely burned
	MG-U					55	Poor	Unburned
AL (Alongshan)	AL-S	51.88 68	121.90 67	669	Larch forest	25	Moderately good	Severely burned
	AL-U					55	Poor	Unburned

GL (Gulian)	GL-S	53.04	122.05	582	Shrub wetland	30	Somewhat poor	Severely burned
	GL-U	32	04			60	Poor	Unburned
MH (Mo'he)	MH-S	52.98	122.11	486	Shrub wetland	30	Somewhat poor	Severely burned
	MH-U	59	15			60	Poor	Unburned

204 The horizontal distance between MG-U and MG-S was about 200 m, with the MG-
205 U on the edge of the burned area. Observations of ground temperatures began in
206 February 2017 (two years after fire). At MG-U in the Xing'an larch (*Larix gmelinii*)
207 dominated forest, all larch trees at MG-S were burned to death, and low shrubs and
208 herbs were found in 2022. The horizontal distance between AL-U and AL-S was less
209 than 100 m, with the AL-U on the edge of the burned area. Observations of ground
210 temperatures began in February 2017 (eight years after fire). The vegetation was the
211 Xing'an larch forest at AL-U, and; it was the broad-leaved forest (birch) at AL-S. We
212 selected GL-S and GL-U sites about 2 km apart from each other. Measurements of
213 ground temperatures began in February 2017 (15 years after fire). The vegetation was
214 the shrub wetland at GL-U and GL-S. MH-S and MH-U sites were about 5 km apart.
215 Observations of ground temperatures began in February 2017 (30 years after fire). The
216 ecosystem was characteristic of shrub wetlands at MH-U and MH-S.

217 2.2 Fire severity

218 Normalized Burn Ratio (NBR) and differential Normalized Burn Ratio (dNBR)
219 are often used to assess the forest fire severity (Cocke et al., 2005; Li et al., 2022b), and
220 the calculation formulas are as follows:

$$221 \quad NBR = (\rho_{NIR} - \rho_{MIR}) / (\rho_{NIR} + \rho_{MIR}) \quad (1)$$

$$222 \quad dNBR = NBR_{prefire} - NBR_{postfire} \quad (2)$$

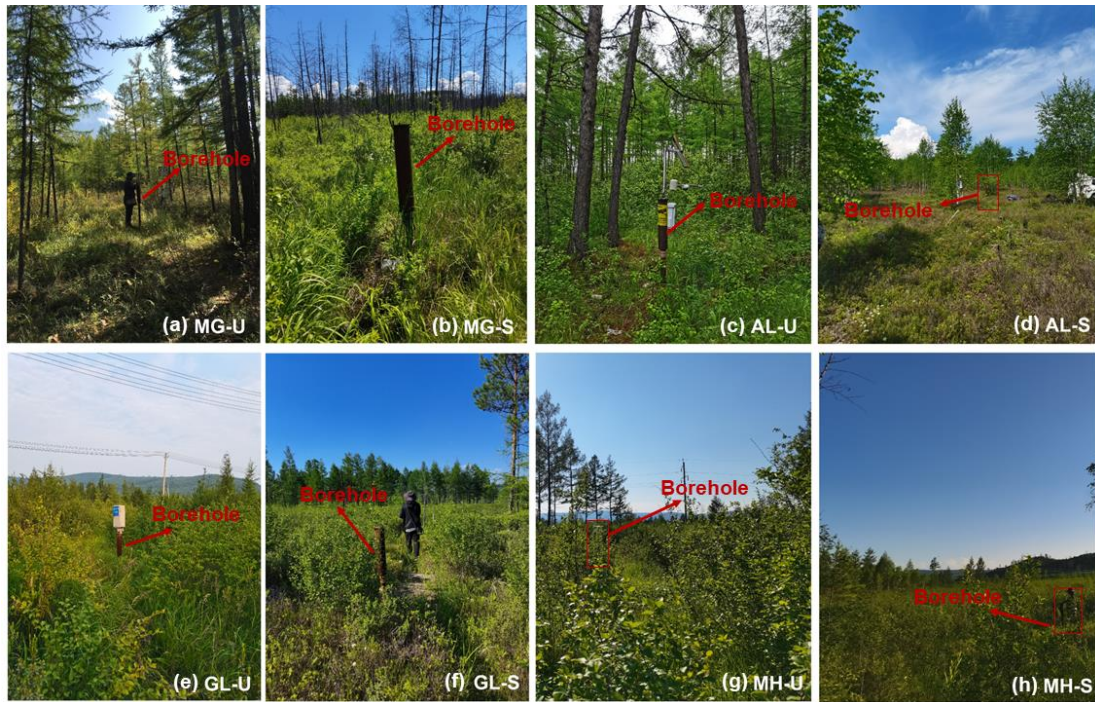
223 where ρ_{NIR} and ρ_{MIR} are the reflectivity values of pixel from the near-infrared (NIR)
224 and middle-infrared (MIR) bands, and; $NBR_{prefire}$ and $NBR_{postfire}$ are the values
225 of NBR before and after fire.

226 According to the values of $dNBR$, fire severity is divided into four categories:

227 severely burned ($\text{dNBR} \geq 0.571$), moderately burned (0.241-0.570), lightly burned
228 (0.051-0.240), and unburned (≤ 0.050) (Cocke et al., 2005). In the lightly and
229 moderately burned areas, there were difficulties in drilling and/or monitoring due to
230 device malfunction or damage. In addition, the permafrost environment changes more
231 significantly after severe burns. Therefore, only sites of two levels of fire severity
232 (severely burned and unburned) were chosen for the abovementioned four areas
233 (Mangui/MG, Alongshan/AL, Gulian/GL and Mo'he/MH) to study post-fire changes in
234 ground hydrothermal regimes and soil nutrients.

235 **2.3 Site instrumentation and laboratory analysis**

236 At each site of unburned and severe burned, a 20-m-deep borehole was drilled and
237 instrumented in October 2016 to monitor ground temperatures (eight boreholes in total)
238 (Figure 2). Ground temperatures were monitored with 0.5-m depth intervals at depths
239 of 0–5 m and then with 1-m depth intervals at depths of 5-20 m by thermistor cables
240 permanently installed in boreholes and manually measured from February 2017. All
241 thermistors were assembled and calibrated at the Key Laboratory of Cryospheric
242 Science and Frozen Soil Engineering, Northwest Institute of Eco-Environment and
243 Resources (renamed from the merger of the former State Key Laboratory of Frozen Soil
244 Engineering and the State Key Laboratory of Cryosphere Science, Cold and Arid
245 Regions Environmental and Engineering Research Institute), Chinese Academy of
246 Sciences. Since February 2017, ground temperatures at these boreholes were manually
247 measured thrice monthly (Table 2), or occasionally once or twice monthly due to traffic
248 difficulty or control, by a multi-meter Fluke 189[®] device. According to the measured
249 soil temperatures during the observation period, the isotherms of soil temperature in the
250 vertical profile at depths of 0-20 m were drawn, and then the 0°C isotherms were
251 delineated for each borehole. The values of ALT were then determined, using linear
252 extrapolation of seasonally and progressively changing ground temperature distribution
253 with depth, for each borehole and each year according to the deepest position of the 0°C
254 isotherms in the year.



255

256 Figure 2. Photos of the study sites with different vegetation cover and the position of the 20 m deep
 257 boreholes for monitoring the ground temperature in the northern Da Xing'anling Mountains in
 258 Northeast China in 3-5 July 2022.

259 Notes: Figures 2a and 2b were the borehole for observation of ground temperature at Xing'an larch
 260 forest severe burned and light burned sites in MG; Figures 2c and 2d were the borehole for
 261 observation of ground temperature in a Xing'an larch forest at severe burned and light burned sites
 262 in AL; Figures 2e and 2f were the borehole for observation of ground temperature in shrub wetlands
 263 at severe burned and light burned sites in GL; Figures 2g and 2h were the borehole for observation
 264 of ground temperature at shrub wetlands severe burned and light burned sites in MH.

265 Table 2. Monitoring data for the eight sites of soil nutrients and ground temperature boreholes for studying fire impacts on the permafrost environment in the northern
 266 Da Xing'anling Mountains in Northeast China

Study sites	Monitoring depths (m)			Time period	Monitoring frequency
	Soil nutrients	Soil gravimetric moisture content (SMC)	Ground temperature		
MG-U	0.1, 0.2, 0.3, 0.4, 0.5, 0.6, 0.7, 0.8, 0.9, 1.0, 1.1, 1.2, 1.3, 1.4, 1.5, 1.6, 1.7, 1.8, 1.9, 2.0, 2.1, 2.2, 2.3, 2.4, 2.5	0.2, 0.3, 0.4, 0.5, 0.6, 0.7, 0.8, 0.9, 1.0, 1.1, 1.2, 1.3, 1.4, 1.5, 1.6, 1.7, 2.0, 2.5, 2.7	0.0, 0.2, 0.5, 1.0, 1.5, 2.0, 2.5, 3.0, 3.5, 4.0, 5.0, 6.0, 7.0, 8.0, 9.0, 10.0, 11, 12, 13, 14, 15, 16, 17, 18, 19, 20	2016; 2016; 2017-2022	Once; Once; Thrice/ month
MG-S	0.1, 0.2, 0.3, 0.4, 0.5, 0.6, 0.7, 0.8, 0.9, 1.0, 1.1, 1.2, 1.3, 1.4, 1.5, 1.6, 1.7, 1.8, 1.9, 2.0, 2.1, 2.2, 2.3, 2.4, 2.5, 2.6	0.2, 0.3, 0.4, 0.5, 0.6, 0.7, 0.8, 0.9, 1.0, 1.1, 1.2, 1.3, 1.4, 1.5, 1.6, 1.7, 1.8, 1.9, 2.0, 2.1, 2.2, 2.6, 4.6, 5.6, 6.1, 7.6	0.0, 0.2, 0.5, 1.0, 1.5, 2.0, 2.5, 3.0, 3.5, 4.0, 5.0, 6.0, 7.0, 8.0, 9.0, 10.0, 11, 12, 13, 14, 15, 16, 17, 18, 19, 20	2016; 2016; 2017-2022	Once; Once; Thrice/ month
AL-U	0.1, 0.2, 0.3, 0.4, 0.5, 0.6, 0.7, 0.8, 0.9, 1.0, 1.1, 1.2, 1.3, 1.4, 1.5, 1.6, 1.7, 1.8, 1.9, 2.0, 2.1, 2.2, 2.3, 2.4, 2.5, 2.6, 2.7, 2.8, 2.9, 3.0	0.1, 0.2, 0.3, 0.4, 0.5, 0.6, 0.7, 0.8, 0.9, 1.0, 1.1, 1.2, 1.3, 1.4, 1.5, 1.6, 1.7, 1.8, 1.9, 2.0, 2.1, 2.2, 2.3, 2.4, 2.5, 2.6, 2.7, 2.8, 2.9, 3.0, 3.1, 3.2, 3.5, 4.0, 4.5, 5.0, 5.5, 5.9, 6.4, 9.4	0.0, 0.2, 0.5, 1.0, 1.5, 2.0, 2.5, 3.0, 3.5, 4.0, 5.0, 6.0, 7.0, 8.0, 9.0, 10.0, 11, 12, 13, 14, 15, 16, 17, 18, 19, 20	2016; 2016; 2017-2022	Once; Once; Thrice/ month
AL-S	0.1, 0.2, 0.3, 0.4, 0.5, 0.6, 0.7, 0.8, 0.9, 1.0, 1.1, 1.2, 1.3, 1.4, 2.1, 2.2, 2.3, 2.4, 2.5, 2.6, 2.7, 2.8	0.2, 0.3, 0.4, 0.5, 0.6, 0.7, 0.8, 0.9, 1.1, 1.4, 1.5, 1.7, 2.0, 2.2, 2.4, 2.6, 2.8, 2.9, 3.1, 3.4, 3.6, 4.0, 4.1, 4.5, 4.8, 5.5, 6.0, 7.0, 7.5	0.0, 0.2, 0.5, 1.0, 1.5, 2.0, 2.5, 3.0, 3.5, 4.0, 5.0, 6.0, 7.0, 8.0, 9.0, 10.0, 11, 12, 13, 14, 15, 16, 17, 18, 19, 20	2016; 2016; 2017-2022	Once; Once; Thrice/ month
GL-U	0.1, 0.2, 0.3, 0.4, 0.5, 0.6, 0.7, 0.8, 0.9, 1.0, 1.1, 1.4, 1.5, 1.6, 1.7, 1.8, 1.9, 2.0, 2.1, 2.2, 2.3, 2.4, 2.5, 2.6, 2.7, 2.8, 2.9, 3.0, 3.1, 3.4, 3.5, 3.6	0.1, 0.2, 0.3, 0.4, 0.5, 0.6, 0.7, 0.8, 0.9, 1.0, 1.1, 1.3, 1.4, 1.5, 1.6, 1.7, 1.8, 1.9, 2.0, 2.7, 2.8, 2.9, 3.0, 3.1	0.0, 0.2, 0.5, 1.0, 1.5, 2.0, 2.5, 3.0, 3.5, 4.0, 5.0, 6.0, 7.0, 8.0, 9.0, 10.0, 11, 12, 13, 14, 15, 16, 17, 18, 19, 20	2016; 2016; 2017-2022	Once; Once; Thrice/ month
GL-S	0.1, 0.2, 0.3, 0.4, 0.5, 0.6, 0.7, 0.8, 0.9, 1.0, 1.2, 1.3, 1.4, 1.5, 2.0, 2.1, 2.2, 2.4, 2.5, 2.6, 2.7, 2.8	0.1, 0.2, 0.3, 0.8, 2.0, 2.4, 2.7, 3.6, 4.2, 4.7, 5.6, 8.4	0.0, 0.2, 0.5, 1.0, 1.5, 2.0, 2.5, 3.0, 3.5, 4.0, 5.0, 6.0, 7.0, 8.0, 9.0, 10.0, 11, 12, 13, 14, 15, 16, 17, 18, 19, 20	2016; 2016; 2017-2022	Once; Once; Thrice/ month
MH-U	0.1, 0.2, 0.3, 0.4, 0.5, 0.6, 0.7, 0.8, 0.9, 1.0, 1.1, 1.4, 1.5, 1.6, 1.7, 1.8, 1.9, 2.0, 2.1, 2.2, 2.3, 2.4, 2.5, 2.6, 2.7, 2.8, 2.9, 3.0, 3.1, 3.4, 3.5, 3.6	0.1, 0.2, 0.3, 0.4, 0.5, 0.6, 0.7, 0.8, 0.9, 1.0, 1.1, 1.3, 1.4, 1.5, 1.6, 1.7, 1.8, 1.9, 2.0, 2.7, 2.8, 2.9, 3.0, 3.1	0.0, 0.2, 0.5, 1.0, 1.5, 2.0, 2.5, 3.0, 3.5, 4.0, 5.0, 6.0, 7.0, 8.0, 9.0, 10.0, 11, 12, 13, 14, 15, 16, 17, 18, 19, 20	2016; 2016; 2017-2022	Once; Once; Thrice/ month
MH-S	0.1, 0.2, 0.3, 0.4, 0.5, 0.6, 0.7, 0.8, 0.9, 1.0, 1.1, 1.2, 1.3, 1.4, 1.5, 1.6, 1.7, 1.8, 1.9, 2.0	0.1, 0.2, 0.3, 0.4, 0.5, 0.6, 0.7, 0.8, 0.9, 1.0, 1.1, 1.2, 1.3, 1.4, 1.5, 1.6, 1.7, 1.8, 1.9, 2.0, 2.3, 3.6	0.0, 0.2, 0.5, 1.0, 1.5, 2.0, 2.5, 3.0, 3.5, 4.0, 5.0, 6.0, 7.0, 8.0, 9.0, 10.0, 11, 12, 13, 14, 15, 16, 17, 18, 19, 20	2016; 2016; 2017-2022	Once; Once; Thrice/ month

267 Notes: Soil nutrients and SMC were observed once in 2016, and soil temperatures were observed thrice monthly in 2017-2022.

268 While drilling in 2016, soil samples were collected from depths of 0-9.4 m at
269 intervals of 0.1-3.0 m, with a total of 402 soil samples. Three replicas were collected at
270 the same depth and then three samples were evenly mixed into one. At depths of 0-3.0
271 m, samples were collected every 10 cm in depth in soil strata with more significant
272 changes of soil organic matter and lithology near the ground surface. At depths of 3.0-
273 9.4 m, samples were collected based on lithological similarity or changes in soil or rock
274 strata, rather than at an equal depth interval of 0.1 m. Therefore, at depths of 0-3 m,
275 there were generally a set of data at a regular depth interval of 10 cm, but at depths of
276 3-10 m, the depth intervals of datasets varied substantially. One part of the soil samples
277 was collected using a cutting ring and stored in an 100-cm³ aluminum specimen box
278 and immediately weighed (soil wet weight). Then, the samples were transported to the
279 laboratory and dried at 105°C to obtain soil dry weight. Finally, gravimetrically-based
280 SMC was calculated by the mass of soil before and after drying. The other part of the
281 soil samples was collected and stored in zip-lock bags and timely brought back to the
282 laboratory for air-drying, then passed through a 2-mm sieve for chemical analysis. SOC
283 and TN contents were measured by potassium dichromate oxidation reduction and
284 Kjeldahl nitrate boiling fluid injection methods, respectively (Nelson et al., 1982). TP
285 and TK contents were determined by the methods of Mo-Sb colorimetry and flame
286 photometry, respectively (Sun et al., 2011). These data are shown as mean ± standard
287 error (SE). Changes in ground temperatures and soil chemical properties were analyzed
288 using the space-for-time chronosequence approach (Mack et al., 2021).

289 **2.4 Data quality check**

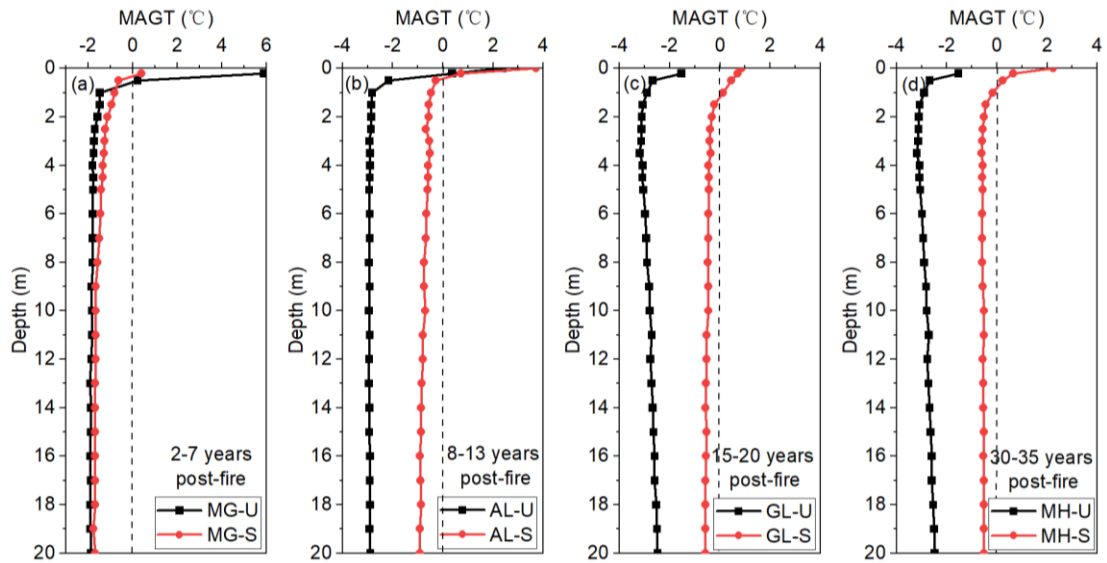
290 The measurement accuracy of ground temperature was ±0.05°C in the range of
291 -30 to +30°C, but ± 0.1°C in those of -45 to -30°C and +30 to +50°C. From 2020 to
292 2022, due to the breakout and persistence of the COVID-19 epidemic, some data were
293 not timely collected, affecting the sampling intervals. Ground temperature data were
294 collected manually thrice monthly since February 2017, and after the outbreak of the
295 COVID-19 pandemic, the data were recorded once or twice monthly. In addition, some
296 data were missing because of damaged, broken, or destroyed probes, solar panel

297 batteries, or dataloggers. From 6 February 2017 to 22 November 2022, a total of 28,890
298 pieces of data were collected, of which 178 NA (not available) data were resulted from
299 probe damage, thus 28,712 valid data were collected. All the missing data were near
300 the ground surface, at a soil layer at depths between 0 and 5 cm. At MG-U, AL-U, AL-
301 S, GL-S, and MH-S, all data were available. Of the 178 NA data, 74 were at MG-S
302 (from 17 September 2019 to 22 November 2022), 52 at GL-U (from 20 July 2019 to 13
303 February 2022), and 52 at MH-U (from 20 July 2019 to 13 February 2022) sites. Data
304 of soil temperatures from manually monitored boreholes were quality-controlled for
305 each measurement. Some studies have also shown that this method of monitoring
306 ground temperature using drilling and probes is one of the most accurate, reliable, and
307 intuitive methods for long-term monitoring of permafrost data (Chang et al., 2022; Li
308 et al., 2022a, 2024; Zhao et al., 2021). Before the analysis of soil nutrient data and SMC
309 data, we conducted outlier tests to ensure the accuracy of the data. These tests showed
310 that all the data have no outliers and the samples are representative. There was a total
311 of 840 soil nutrient data and 195 SMC data.

312 **3 Data descriptions and evaluation**

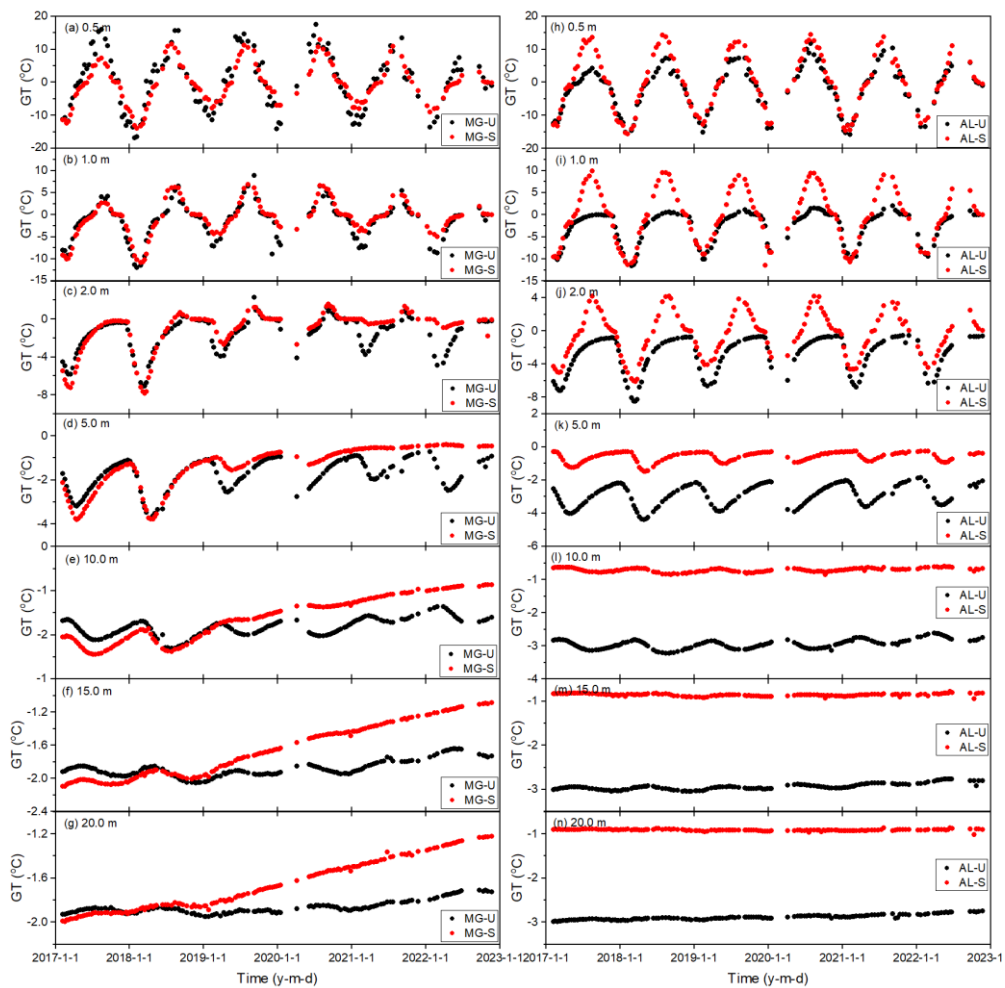
313 **3.1 Changes in ground temperatures of near-surface permafrost**

314 Ground temperatures at depths of 0-20 m in the active layer and near-surface
315 permafrost showed remarkable seasonal dynamics (Figures 3 and 4). The amplitudes of
316 changes in ground temperature decreased exponentially with increasing depth. At
317 depths of 0-1 m, changes in MAGT at eight sites were larger 1.5-10.2°C than those at
318 1-20 m (Figures 3a to 3d).



319
320
321
322

Figure 3. Mean annual ground temperatures (MAGTs) from 2017 to 2022 at the unburned and severely burned sites in the four areas on the western flank of the northern Da Xing'anling Mountains in Northeast China



323
324
325
326

Figure 4. Variability of ground temperatures at depths of 0–20 m at Xing'an larch forest sites in Mangui (MG) and Alongshan (AL) on the western flank of the northern Da Xing'anling Mountains in Northeast China during the period from 2017 to 2022.

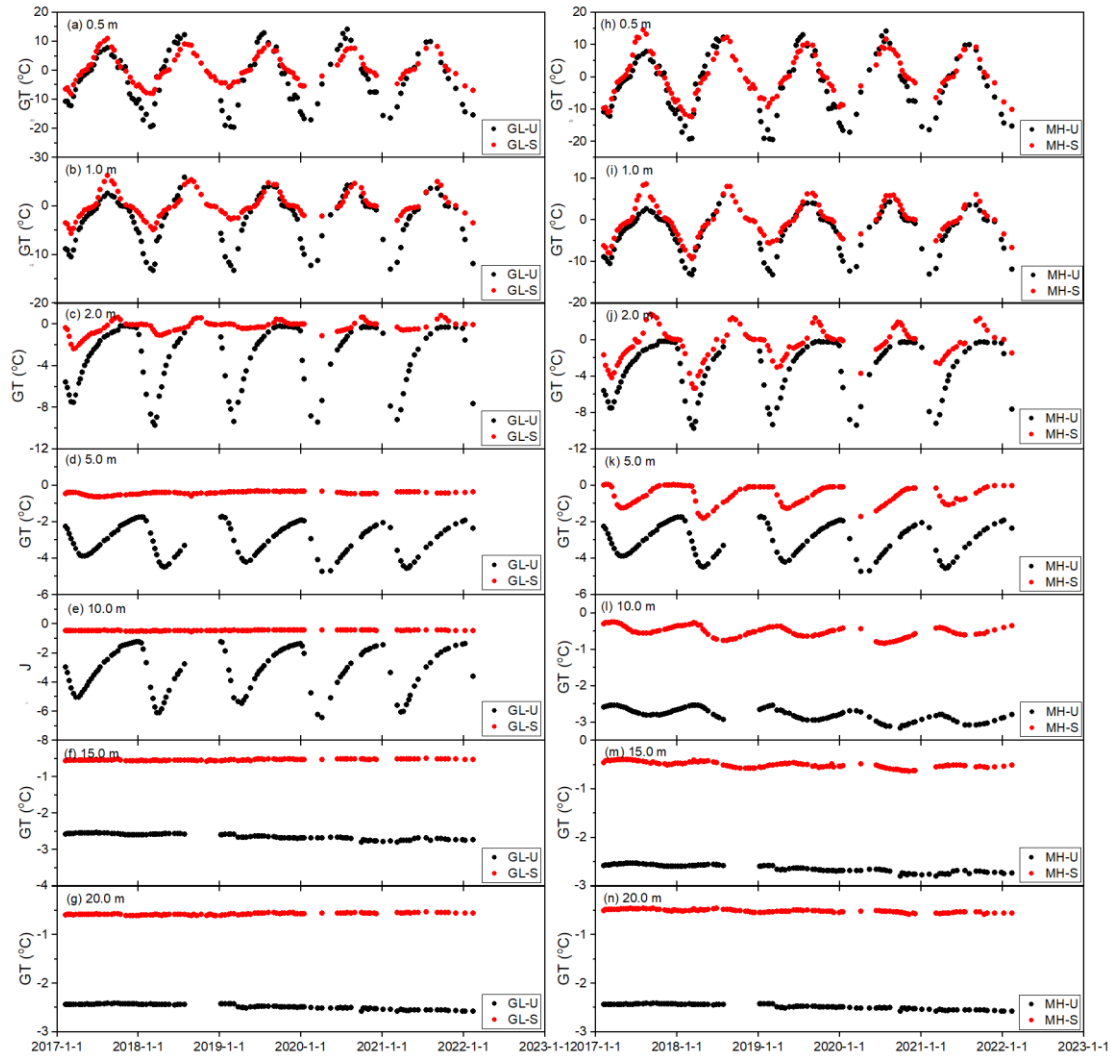
327 Notes: The symbol U stands for the unburned site, S for the severely burned site, and; GT, for ground
 328 temperature. Figures 4a to 4g were the changes in ground temperatures in Mangui (MG) 2 to 7 years
 329 after fire; Figures 4h to 4n, those in Alongshan (AL) 8 to 13 years after fire.

330 MAGTs lowered with increasing depths, the temperature difference between 0.5
 331 and 20 m in depth was 0.2-2.1°C (Table 3). From 2017 to 2022, ground temperature
 332 fluctuated in a sinusoidal pattern at depths of 0.5 to 2.0 m, and this dynamic change
 333 gradually disappeared with increasing depth (Figures 3a to 3g and 5a to 5g). At the
 334 depth of 5 m, ground temperature was subzero or cryotic perennially (Figures 4d, 4k,
 335 5d, and 5k). At eight sites, from 2017 to 2022, ground temperatures showed an
 336 increasing trend of 0.01-0.69°C/yr at depths of 0.5-20 m. The increase rate was the
 337 largest at AL-U (0.03-0.69°C/yr), and; the lowest, at AL-S and GL-S (all were 0.01-
 338 0.37°C/yr) (Figures 4a to 4g and Figures 5a to 5g).

339 Table 3. Mean annual ground temperatures (MAGTs) at each of the seven measured depths at
 340 unburned and severely burned sites in the four areas on the western flank of the northern Da
 341 Xing'anling Mountains in Northeast China during the period from 2017 to 2022

Depth (m)	0.5		1.0		2.0		5.0		10		15		20	
Fire severity	U	S	U	S	U	S	U	S	U	S	U	S	U	S
MG	0.2	-0.6	-1.5	-0.8	-1.6	-1.1	-1.7	-1.4	-1.8	-1.6	-1.9	-1.7	-1.9	-1.7
AL	-2.2	-0.3	-2.8	-0.5	-2.9	-0.6	-2.9	-0.6	-2.9	-0.7	-2.9	-0.9	-2.9	-0.9
GL	-2.7	0.5	-2.9	0.1	-3.1	-0.3	-3.1	-0.4	-2.8	-0.5	-2.6	-0.5	-2.5	-0.6
MH	-2.7	0.2	-2.9	-0.2	-3.1	-0.5	-3.1	-0.6	-2.8	-0.5	-2.6	-0.5	-2.5	-0.5

342 Notes: U stands for unburned sites, and; S, severely burned sites.



343

344 Figure 5. Variations in ground temperatures at depths of 0-20 m at shrub wetlands sites in Gulian
 345 (GL) and Mo'he (MH) on the western flank of the northern Da Xing'anling Mountains in Northeast
 346 China during the period from 2017 to 2022.

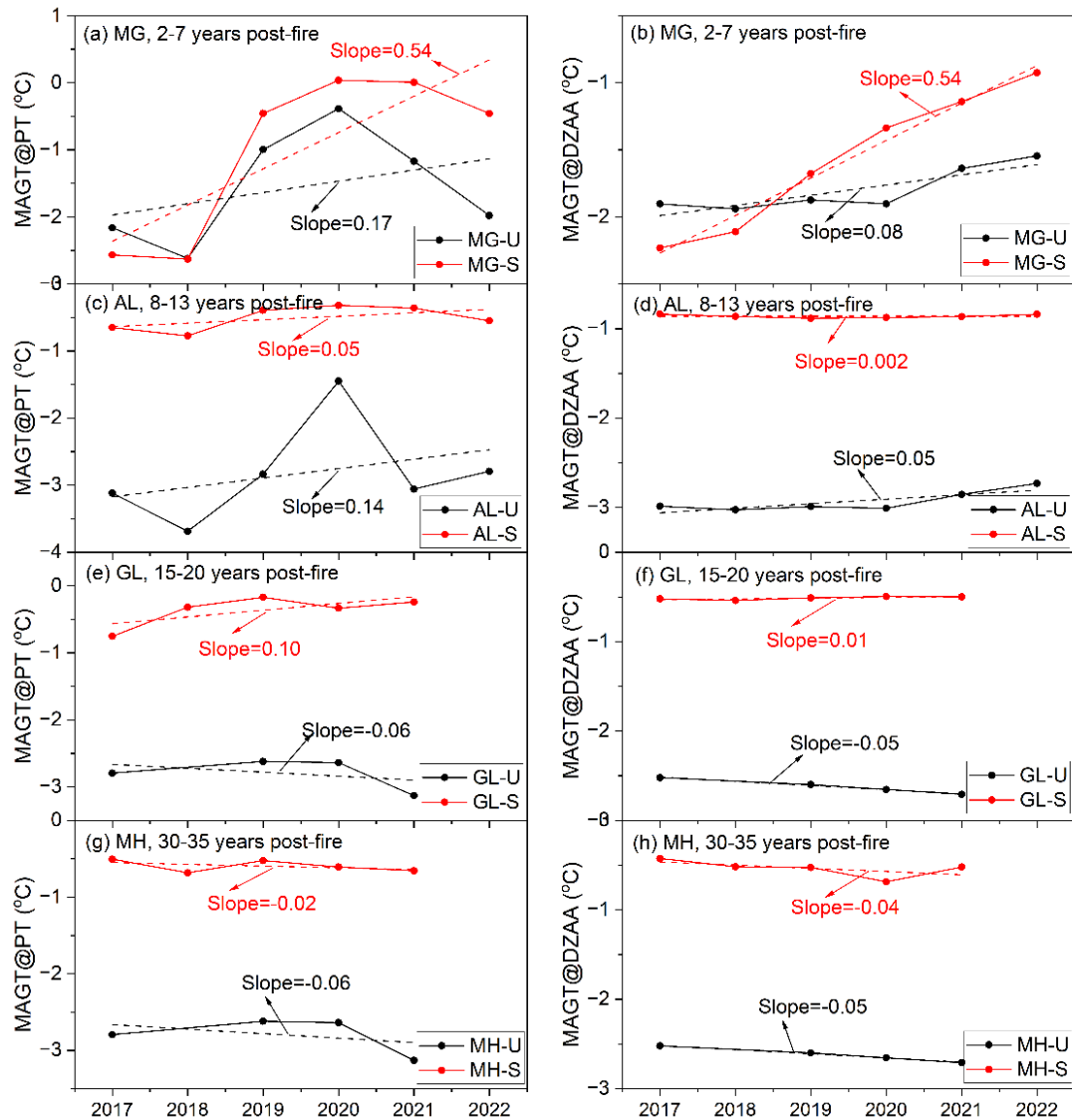
347 Notes: The symbol U stands for the unburned site; S, for the severely burned site, and; GT, for
 348 ground temperature. Figures 5a to 5g were changes in ground temperatures in GL 15-20 years after
 349 fire; Figures 5h to 5n, those in MH 30-35 years after fire.

350 3.2 Changes in MAGTs at the permafrost table ($MAGT_{PT}$) and D_{ZAA} ($MAGT_{DZAA}$)

351 $MAGT$ s at the permafrost table ($MAGT_{PT}$) and at the D_{ZAA} ($MAGT_{DZAA}$) can truly
 352 reflect the changing characteristics of permafrost thermal regimes. Therefore, in this
 353 section, we have chosen $MAGT_{PT}$ and $MAGT_{DZAA}$ to briefly analyze changes in ground
 354 thermal regimes. When the temperature probe was missing at the actual depth of the

355 permafrost table or the D_{ZAA} , $MAGT_{PT}$ and $MAGT_{DZAA}$ were derived from
356 interpolation of adjacent ground temperatures.

357 At the eight monitored sites, the burial depths of permafrost table ranged between
358 1.5 and 4.5 m, and the D_{ZAA} between 10 and 16 m. From 2017 to 2022, except for GL-
359 U, MH-U and MH-S sites, $MAGT_{PT}$ and $MAGT_{DZAA}$ decreased gradually (-0.02 to
360 $-0.06^{\circ}\text{C}/\text{yr}$), while at other sites increased at rates of 0.01 - $0.54^{\circ}\text{C}/\text{yr}$ (Figure 6). The
361 ground warming rates of $MAGT_{PT}$ and $MAGT_{DAZZ}$ were highest at the MG-S site (both
362 at $0.54^{\circ}\text{C}/\text{yr}$), and lowest at the GL-S site (0.10 and $0.01^{\circ}\text{C}/\text{yr}$) (Figures 6a and 6b).
363 From 2017-2022, the highest differences in $MAGT_{PT}$ and $MAGT_{DAZZ}$ were 2.6 and 1.3°C
364 at the MG-S site, respectively, and the lowest were 0.2 and 0.1°C at MH-S and AL-S
365 sites, respectively (Figures 6a, 6d and 6h).



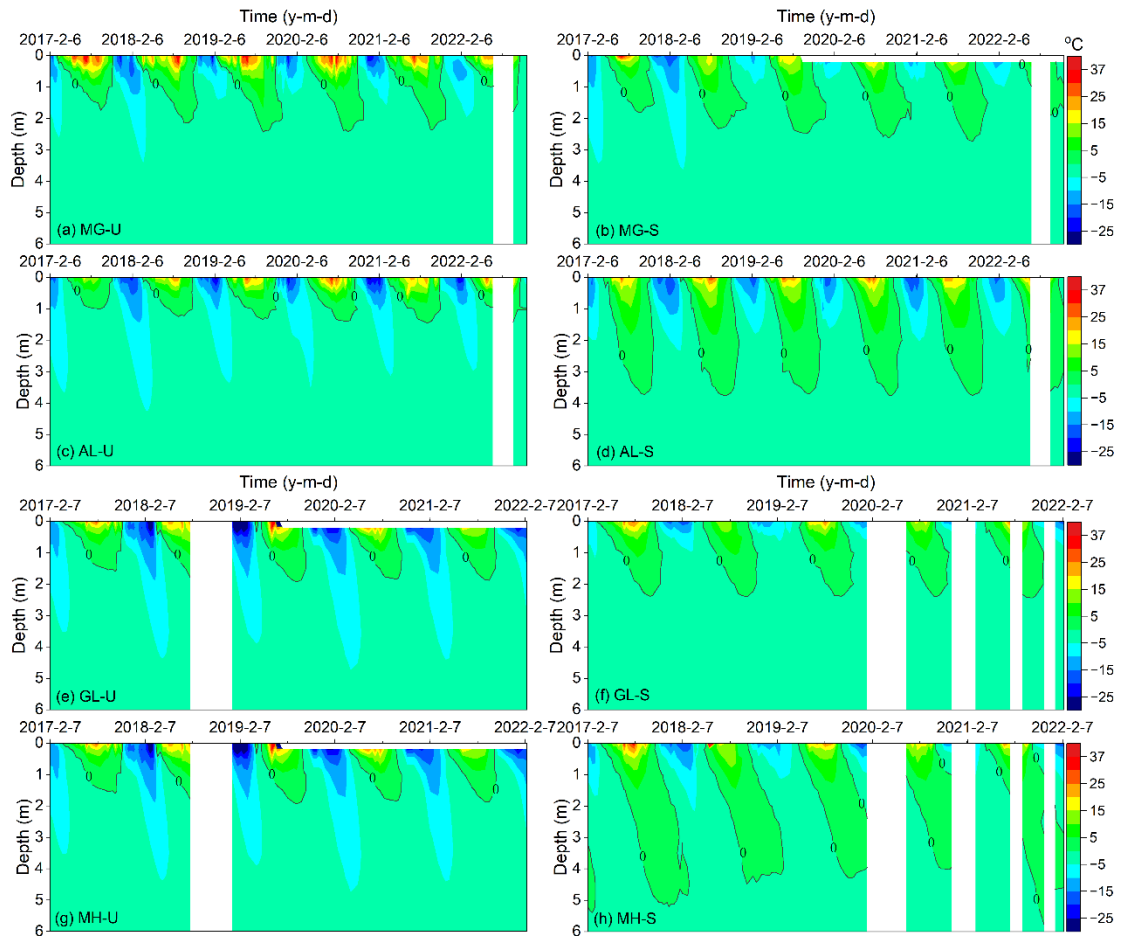
366

367 Figure 6. Variations in mean annual ground temperatures at the permafrost table (MAGT_{PT}) and the
 368 depth of zero annual amplitude (D_{ZAA}) (MAGT_{DZAA}) at eight sites in the four study areas (Mangui
 369 or MG, Alongshan or AL, Gulian or GL, and Mo'he or MH) on the western flank of the northern
 370 Da Xing'anling Mountains in Northeast China during 2017-2022.

371 Notes: U stands for unburned sites, and; S, severely burned sites.

372 3.3 Active layer thickness (ALT) data

373 ALT, defined as the annual maximum depth of seasonal thaw penetration, was
 374 determined according to the deepest position of the 0°C isotherms in a year. Although
 375 some data were missing, the change trends of ALT were still obvious (Figure 7).

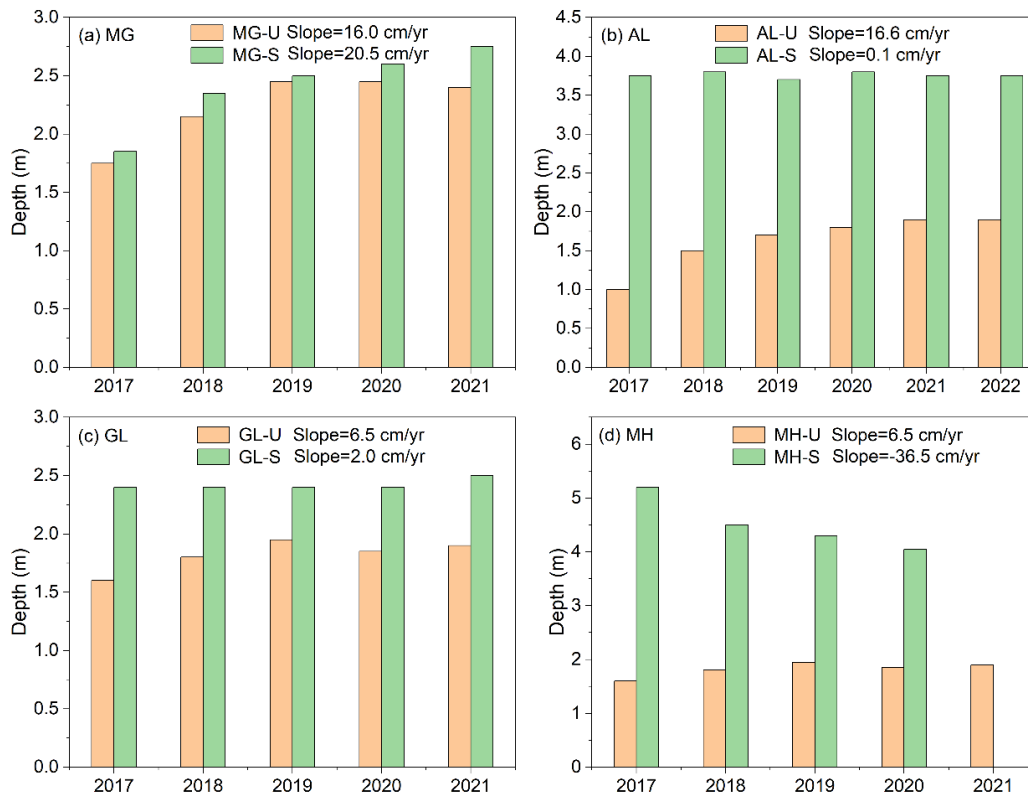


376

377 Figure 7. Variability of ground temperatures isotherms at eight sites in Mangui (MG), Alongshan
 378 (AL), Gulian (GL), and Mo'he (MH) on the western flank of the northern Da Xing'anling Mountains
 379 in Northeast China during 2017-2022.

380 Notes: U stands for the unburned sites, as in insets a (site MG-U), c (site AL-U), e (site GL-U), and
 381 g (site MH-U), and S, the severely burned sites, as in insets b (site MG-S), d (site AL-S), f (site GL-
 382 S), and h (site MH-S).

383 ALT was between 1.0 and 5.2 m at the eight sites from 2017 to 2022, and the
 384 maximum average of ALT was 4.5 m at MH-U and the minimum was 1.6 m at AL-U.
 385 Compared with the other seven sites, MH-S has the largest ALT, with a maximum of
 386 5.2 m in 2017. From 2017 and 2022, only at the MH-S site, ALT decreased at a rate of
 387 36.5 cm/yr, while at the other sites it increased at rates of 0.1-20.5 cm/yr. The increase
 388 rate of ALT at MG-S was the fastest, and; at AL-S, the slowest (Figure 8).



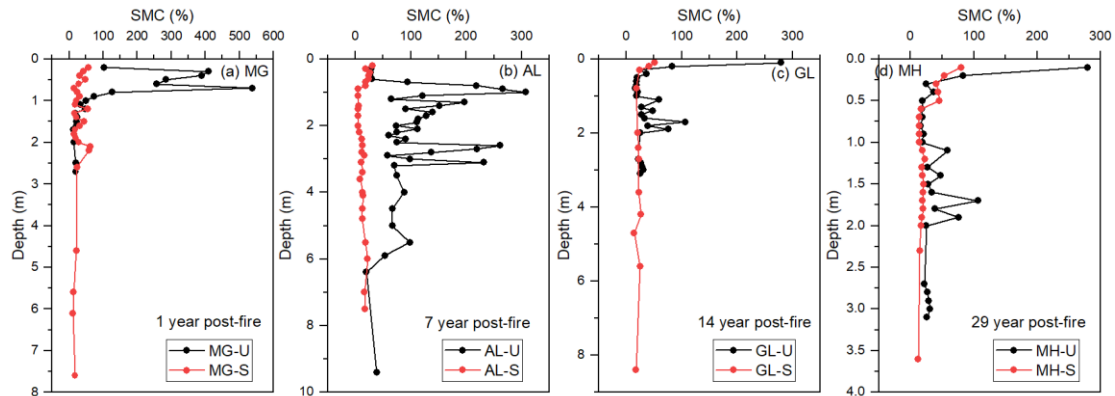
389

390 Figure 8. Variation characteristics of active layer thickness (ALT) from 2017 to 2022 at eight sites
 391 of the four study areas in Mangui (MG), Alongshan (AL), Gulian (GL), and Mo'he (MH) on the
 392 western flank of the northern Da Xing'anling Mountains in Northeast China during 2017-2022.
 393 Notes: U stands for the unburned site, and S, the severely burned site.

394 3.4 Variations in gravimetric soil moisture content (SMC)

395 At MG-U and AL-U sites, SMC decreased with increasing depth, especially in the
 396 active layer and near-surface permafrost, or in the vicinity of the permafrost table
 397 (Figure 9). For example, at AL-U, SMC decreased at a rate of 8.6%/m and average
 398 SMC was $108.2 \pm 11.7\%$ at depths of 0-9.4 m (Figure 9b). At the depths (0-3 m) with
 399 higher SMC, the soil contains massive ice crystals and a large amount of segregated ice,
 400 with ice lenses of 0.1–5.0 cm in thickness. For example, at GL-U, SMC was higher at
 401 the junction of the bottom of the active layer and the upper layer of transient permafrost
 402 (1-2 m in depth) due to a large amount of segregated ice (0.2-5.0 cm thick) immediately
 403 under the permafrost table. At MG-S, AL-S, GL-S, and MH-S sites, changes in SMC

404 were inconspicuous, only at depths of 0-0.5 m, with a slight decreasing trend. At depths
 405 of 0.5-9.4 m, differences in SMC were minor (Figure 9). At MG-S, SMC fluctuated
 406 between 11.7-63.2% at depths of 0.6-7.6 m, with average SMC at $27.5\pm 3.2\%$ (Figure
 407 9a). At AL-S, GL-S, and MH-S sites, SMC fluctuated between 4.7-26.6% at depths of
 408 0.6-8.4 m, with average SMC of 17.1-21.1%.

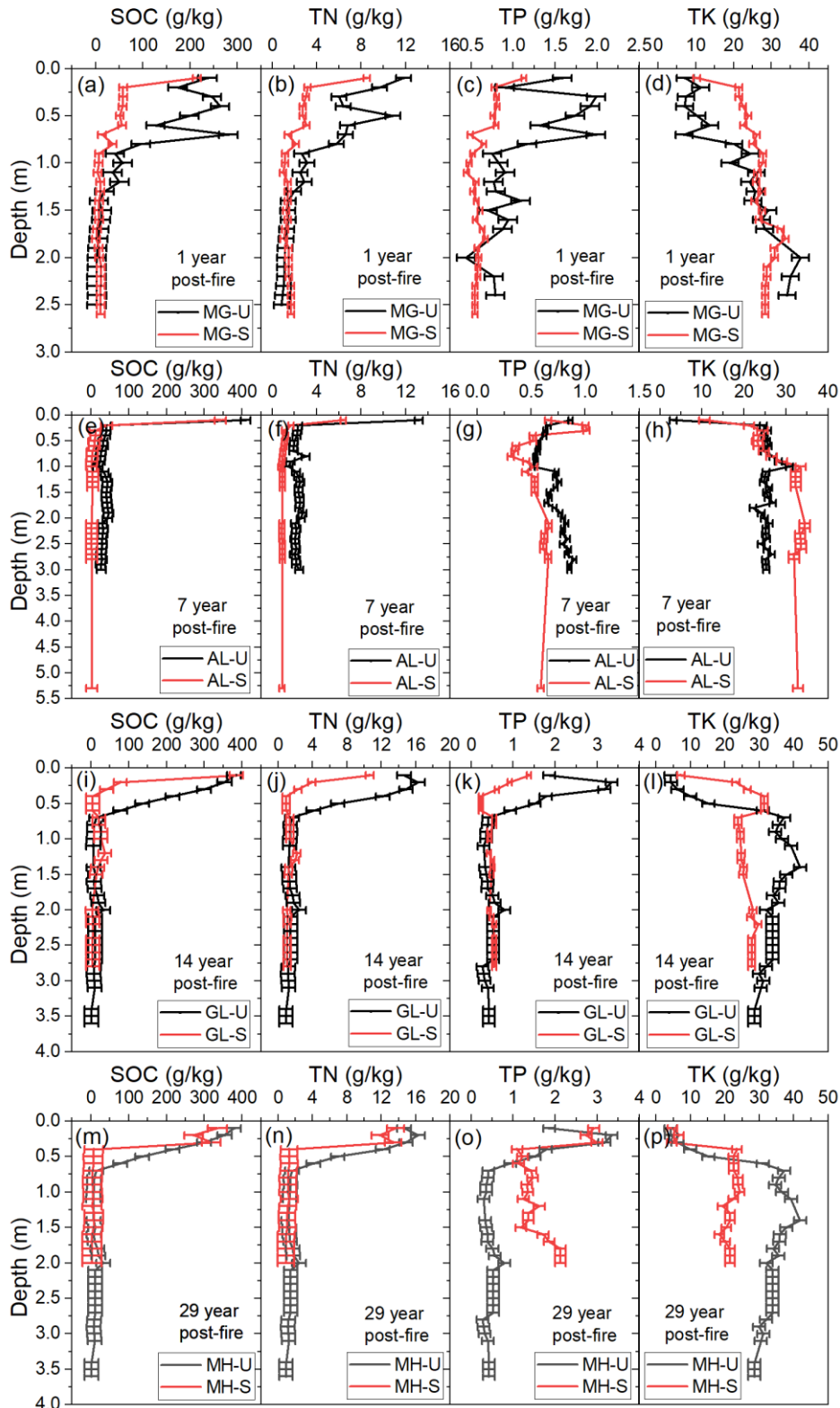


409

410 Figure 9. Variations in gravimetrically-based soil moisture contents (SMC) with different fire severity at eight sites in Mangui (MG), Alongshan (AL), Gulian (GL), and Mo'he (MH) on the
 411 western flank of the northern Da Xing'anling Mountains in Northeast China in 2016. Notes: The
 412 symbol U stands for unburned, S for severely burned, and; SMC, for soil gravimetric moisture
 413 content.
 414

415 3.5 Variations in soil nutrients

416 The contents of SOC and TN decreased with increasing depths. A large amount of
 417 SOC and TN were stored in the active layer (0-1.3 m), especially in the soil organic
 418 layer (0-0.5 m) (Figures 10a to 10n). The change trends of SOC and TN were consistent.
 419 For example, at MG-U, at depths of 0-1.3 m, averages of SOC and TN were 140.5 ± 26.9
 420 and 5.9 ± 0.9 g/kg, respectively; at depths of 1.3-2.5 m, changes in SOC and TN were
 421 relatively smooth, fluctuating between 2.0-13.3 and 0.9-1.5 g/kg, with averages at
 422 5.4 ± 1.1 and 1.2 ± 0.1 g/kg, respectively (Figures 10a and 10b).



423

424 Figure 10. Variations in soil nutrients at eight sites in Mangui (MG, a to d),
 425 Alongshan (AL, e to h), Gulian (GL, i to l), and Mo'he (MH, m to p) on the western flank of the northern Da Xing'anling
 426 Mountains in Northeast China in 2016.

427 Notes: The symbol U stands for unburned, and S for severely burned. SOC stands for soil organic
 428 carbon; TN, for total nitrogen; TP, for total phosphorus, and; TK, for total potassium.

429 TP contents decreased up to 1.0 m in depth, and changes in TP were minor at
430 depths of 1.0-5.3 m (Figures 10c, 10g, 10k, and 10o). For example, at MG-S, TP
431 decreased at a rate of 0.56 g/kg/m at depths of 0-1.0 m, with an average of 0.7 ± 0.1 g/kg
432 (Figure 10c); TP fluctuated between 0.4 and 0.7 g/kg at depths of 1.1-2.6 m, with an
433 average of 0.6 ± 0.01 g/kg. The change trends of TK were opposite with TP because TK
434 contents increased downwards (Figures 10d, 10h, 10l, and 10p). The contents of TK
435 were all below 41.8 g/kg. For example, at MG-U, TK increased at a rate of 14.1 g/kg/m,
436 while TP decreased at a rate of 0.5 g/kg/m (Figures 10c and 10d).

437 **4. Data availability**

438 The dataset of ground temperature, ALT, SMC, SOC, and contents of TN, TP, and
439 TK can be freely downloaded and is available from the National Tibetan Plateau/Third
440 Pole Environment Data Center (<https://doi.org/10.11888/Cryos.tpdc.300933>, Li and Jin,
441 2024). The dataset was classified into three categories: ground temperatures (at MG-U,
442 MG-S, AL-U, AL-S, GL-U, GL-S, MH-U, and MH-S), soil moisture contents (SMCs),
443 and soil nutrient contents (SOC, TN, TP, and TK).

444 **5. Conclusions**

445 The Da Xing'anling (Hinggan) Mountains in Northeast China are located on the
446 southern margin of the Eastern Asia permafrost zone and boreal forest belt. It is an area
447 where fires occur frequently and the thermal state of permafrost is sensitive to fire
448 disturbances. To study fire effects on the permafrost environment, a monitoring network
449 has been established in Northeast China since 2016. Therefore, a long-term field dataset
450 on ground hydrothermal regimes and soil nutrients has been obtained. This dataset fills
451 a gap in a monitoring study of fire effects on the permafrost environment in the
452 hemiboreal forest zone in Northeast China. These data include ground temperatures at
453 depths of 0-20 m, SMC at depths of 0-9.4 m, and contents of SOC, TN, TP, and TK at
454 depths of 0-3.6 m. The data were collected from eight sites in four burned areas (MG
455 in Mangui, AL in Alongshan, GL in Gulian, and MH in Mo'he) with two categories of
456 fire severity (severely burned and unburned) from 2016 to 2022.

457 Long-term monitoring data in the northern Da Xing'anling Mountains in Northeast

458 China have shown a degrading permafrost under the disturbances of climate change
459 and frequent forest fires. This is evidenced by increasing ground temperature,
460 thickening active layer, decreasing SMC, and evidently changing soil nutrient contents.
461 The 6-year long dataset presented in this study has a high-quality time series with only
462 a few missing data. This valuable and hard-won dataset of forest fires and permafrost
463 is worth maintaining and improving in the future. This study provides important basic
464 data for the protection of the ecosystem-dominated Xing'an permafrost and herewith
465 boreal permafrost ecosystems. Furthermore, it is useful for more accurate prediction of
466 fire-induced permafrost changes and for more accurate estimating and better-managing
467 soil carbon stocks. It also provides an important reference for the initiatives of carbon
468 neutralization and carbon peaking control and the assessment of infrastructure safety
469 under fire threats.

470 **Author contributions.** XL and HJ designed and conducted this research. XL compiled
471 the dataset, performed the data analysis, and wrote the manuscript. RH, HW, XC, RŞ, and ZT
472 participated in the fieldwork. HJ, QF, QW, DL and RŞ improved the writing. XL prepared the
473 manuscript with contributions from all co-authors.

474 **Competing interests.** The authors declare no conflict of interest.

475 **Disclaimer.** Publisher's note: Copernicus Publications remains neutral with regard to
476 jurisdictional claims in published maps and institutional affiliations.

477 **Acknowledgments.** We would like to thank all the scientists and students who
478 participated in the fieldwork. We thank the two anonymous reviewers and editors for
479 their thorough reviews and insightful comments that improved the paper. We also are
480 grateful to Professor Xin Li for his encouragement, guidelines, and review of the
481 proposal for writing up this paper and preparation of the datasets.

482 **Financial support.** This research has been supported by the National Natural
483 Science Foundation of China (Grant No. 32241032); Heilongjiang Excellent Youth
484 Fund (Grant No. YQ2022D002), and; Fundamental Research Fund for the Central
485 Universities (Grant Nos. 2572023CT01 and 2572021GT08). Raul-David Şerban

486 received funding from the Autonomous Province of Bozen/Bolzano-Department for
487 Innovation, Research and University (Grant No. 13585/2023).

488 **References**

- 489 Biskaborn, B. K., Smith, S. L., Noetzli, J., Matthes, H., Vieira, G., Streletskiy, D. A., Schoeneich, P.,
490 Romanovsky, V. E., Lewkowicz, A. G., Abramov, A., Allard, M., Boike, J., Cable, W. L.,
491 Christiansen, H. H., Delaloye, R., Dickmann, B., Drozdov, D., Eitzmuller, B., Grosse, G.,
492 Guglielmin, M., Ingeman-Nielsen, T., Isaksen, K., Ishikawa, M., Johansson, M., Johannsson, H.,
493 Joo, A., Kaverin, D., Kholodov, A., Konstantinov, P., Kroger, T., Lambiel, C., Lanckman, J. P., Luo,
494 D., Malkova, G., Meiklejohn, I., Moskalenko, N., Oliva, M., Phillips, M., Ramos, M., Sannel, A. B.
495 K., Sergeev, D., Seybold, C., Skryabin, P., Vasiliev, A., Wu, Q., Yoshikawa, K., Zheleznyak, M. and
496 Lantuit, H.: Permafrost is warming at a global scale, *Nat. Commun.*, 10, 264, doi: 10.1038/s41467-
497 018-08240-4, 2019.
- 498 Boyd, M. A., Walker, X. J., Barnes, J., Celis, G., Goetz, S. J., Johnstone, J. F., Link, N. T., Melvin, A. M.,
499 Saperstein, L., Schuur, E. A. G. and Mack, M. C.: Decadal impacts of wildfire fuel reduction
500 treatments on ecosystem characteristics and fire behavior in Alaskan boreal forests, *For. Ecol.*
501 *Manage.*, 546, 121347, doi: 10.1016/j.foreco.2023.121347, 2023.
- 502 Brown, D. R. N., Jorgenson, M. T., Douglas, T. A., Romanovsky, V. E., Kielland, K., Hiemstra, C.,
503 Euskirchen, E. S. and Ruess, R. W.: Interactive effects of wildfire and climate on permafrost
504 degradation in Alaskan lowland forests, *J. Geophys. Res.-Biogeosci.*, 120, 1619-1637, doi:
505 10.1002/2015jg003033, 2015.
- 506 Certini, G.: Effects of fire on properties of forest soils: A review. *Oecologia*, 143(1), 1–10, 2005.
- 507 Chang, X., Jin, H., Zhang, Y., Li, X., He, R., Li, Y., Lü, L. and Wang, H.: Permafrost thermal dynamics
508 at a local scale in northern Da Xing'anling Mountains. *Environ. Res. Lett.*, 19(6), 064014. doi:
509 10.1088/1748-9326/ad42b6, 2024.
- 510 Chang, X., Jin, H., He, R., Zhang, Y., Li, X., Jin, X. and Li, G.: Permafrost changes in the northwestern
511 Da Xing'anling Mountains, Northeast China, in the past decade, *Earth Syst. Sci. Data*, 14, 3947-
512 3959, doi: 10.5194/essd-14-3947-2022, 2022.
- 513 Chen, X., Kang, S., Hu, Y. and Yang, J.: Temporal and spatial analysis of vegetation fire activity in the
514 circum-Arctic during 2001–2020. *Res. Cold Arid Reg.*, 15(1), 48-56,
515 <https://doi.org/10.1016/j.rcar.2023.03.002>, 2023.
- 516 Chen, Y., Kelly, R., Genet, H., Lara, M. J., Chipman, M. L., McGuire, A. D. and Hu, F. S.: Resilience
517 and sensitivity of ecosystem carbon stocks to fire-regime change in Alaskan tundra, *Sci. Total*
518 *Environ.*, 806, 151482, doi: 10.1016/j.scitotenv.2021.151482, 2022.
- 519 Cocke, A. E., Fulé, P. Z. and Crouse, J. E.: Comparison of burn severity assessments using Differenced
520 Normalized Burn Ratio and ground data, *Int. J. Wildl. Fire*, 14, 189-198, 2005.
- 521 Cunningham, C. X., Williamson, G. J. and Bowman, D. M.: Increasing frequency and intensity of the
522 most extreme wildfires on Earth. *Nat. Ecol. Evol.*, 1-6, [https://doi.org/10.1038/s41559-024-02452-](https://doi.org/10.1038/s41559-024-02452-2)
523 [2](https://doi.org/10.1038/s41559-024-02452-2), 2024.
- 524 Dieleman, C. M., Day, N. J., Holloway, J. E., Baltzer, J., Douglas, T. A. and Turetsky, M. R.: Carbon and
525 nitrogen cycling dynamics following permafrost thaw in the Northwest Territories, Canada, *Sci.*
526 *Total Environ.*, 845, 157288, <https://doi.org/10.1016/j.scitotenv.2022.157288>, 2022.
- 527 Fultz, L. M., Moore-Kucera, J., Dathe, J., Davinic, M., Perry, G., Wester, D., Schwilk, D. W. and Rideout-

528 Hanzak, S.: Forest wildfire and grassland prescribed fire effects on soil biogeochemical processes
529 and microbial communities: Two case studies in the semi-arid Southwest, *Appl. Soil Ecol.*, 99, 118-
530 128, doi: 10.1016/j.apsoil.2015.10.023, 2016.

531 Genet, H., McGuire, A. D., Barrett, K., Breen, A., Euskirchen, E. S., Johnstone, J. F., Kasischke, E. S.,
532 Melvin, A. M., Bennett, A., Mack, M. C., Rupp, T. S., Schuur, A. E. G., Turetsky, M. R. and Yuan,
533 F.: Modeling the effects of fire severity and climate warming on active layer thickness and soil
534 carbon storage of black spruce forests across the landscape in interior Alaska. *Environ. Res. Lett.*,
535 8(4), 045016, doi: 10.1088/1748-9326/8/4/045016, 2013.

536 Gu, H., Jin, J., Cheng, X., Wang, E., Zhou, Y. and Chai, Y.: The long-term impacts on chemical properties
537 of *Larix gmelini* forest on the northern slope of greater Hinggan Mountains from a forest fire of
538 varying fire intensity (in Chinese). *J Nat Resour*, 25(7), 1114-1121, 2010.

539 Holloway, J. E., Lewkowitz, A. G., Douglas, T. A., Li, X., Turetsky, M. R., Baltzer, J. L. and Jin, H.:
540 Impact of wildfire on permafrost landscapes: a review of recent advances and future prospects.
541 *Permafr. Periglac. Process.*, 31(3), 371-382, 2020.

542 Jin, H., Li, S., Cheng, G., Wang, S. and Li, X.: Permafrost and climatic change in China, *Glob. Planet*
543 *Change*, 26(4), 387-404, doi: 10.1016/S0921-8181(00)00051-5, 2000.

544 Jin, H., Yu, Q., Lü, L., Guo, D., He, R., Yu, S., Sun, G. and Li, Y.: Degradation of permafrost in the
545 Xing'anling Mountains, northeastern China, *Permafr. Periglac. Process.*, 18(3), 245-258, doi:
546 10.1002/ppp.589, 2007.

547 Jin, H., Wu, Q. and Romanovsky, V.E.: Editorial: Impacts from degrading permafrost, *Adv. Clim. Change*
548 *Res.*, 12(1), 1-5. doi: 10.1016/j.accr.2021.01.007, 2021.

549 Jin, H., Huang, Y., Bense, V. F., Ma, Q., Marchenko, S. S., Shepelev, V. V., Hu, Y., Liang, S., Spektor, V.
550 V., Jin, X., Li, X. and Li X.: Permafrost degradation and its hydrogeological impacts, *Water*, 14(3),
551 372. doi: 10.3390/w14030372, 2022.

552 Jin, H., Yang, D., Makarieva, O. and Tang, L.: Changes in permafrost and snow cover in the Boreal and
553 Arctic zones (BAZ) and their impacts, *Adv. Clim. Change Res.*, 14(2), 157-163. doi:
554 10.1016/j.accr.2023.04.002, 2023.

555 Johnstone, J. F., Chapin III, F. S., Foote, J., Kemmett, S., Price, K. and Viereck, L.: Decadal observations
556 of tree regeneration following fire in boreal forests, *Can. J. For. Res.*, 34(2), 267-273, doi:
557 10.1139/x03-183, 2004.

558 Johnstone, J. F., Hollingsworth, T. N., Chapin III, F. S. and Mack, M. C.: Changes in fire regime break
559 the legacy lock on successional trajectories in Alaskan boreal forest, *Glob. Change Biol.*, 16(4),
560 1281-1295, doi: 10.1111/j.1365-2486.2009.02051.x, 2010.

561 Jones, B. M., Grosse, G., Arp, C. D., Miller, E., Liu, L., Hayes, D. J. and Larsen, C. F.: Recent Arctic
562 tundra fire initiates widespread thermokarst development, *Sci. Rep.*, 5, 15865, doi:
563 10.1038/srep15865, 2015.

564 Jorgenson, M. T., Harden, J., Kanevskiy, M., O'Donnell, J., Wickland, K., Ewing, S., Manies, K., Zhuang,
565 Q. L., Shur, Y., Striegl, R. and Koch, J.: Reorganization of vegetation, hydrology and soil carbon
566 after permafrost degradation across heterogeneous boreal landscapes, *Environ. Res. Lett.*, 8, 035017,
567 doi: 10.1088/1748-9326/8/3/035017, 2013.

568 Kirilyanov, A.V., Saurer, M., Siegwolf, R., Knorre, A. A., Prokushkin, A. S., Churakova, O. V., Fonti, M.
569 V. and Büntgen, U.: Long-term ecological consequences of forest fires in the continuous permafrost
570 zone of Siberia. *Environ. Res. Lett.*, 15(3), 034061, <https://doi.org/10.1088/1748-9326/ab7469>,
571 2020.

572 Knicker, H.: How does fire affect the nature and stability of soil organic nitrogen and carbon? A review.
573 *Biogeochemistry* 85(1), 91–118, 2007.

574 Knorr, W., Arneeth, A. and Jiang, L.: Demographic controls of future global fire risk, *Nat. Clim. Change*,
575 6, 781-785, doi: 10.1038/nclimate2999, 2016.

576 Koven, C. D., Schuur, E. A. G., Schädel, C., Bohn, T. J., Burke, E. J., Chen, G., Chen, X., Ciais, P.,
577 Grosse, G., Harden, J. W., Hayes, D. J., Hugelius, G., Jafarov, E. E., Krinner, G., Kuhry, P.,
578 Lawrence, D. M., MacDougall, A. H., Marchenko, S. S., McGuire, A. D., Natali, S. M., Nicolsky,
579 D. J., Olefeldt, D., Peng, S., Romanovsky, V. E., Schaefer, K. M., Strauss, J., Treat, C. C. and
580 Turetsky, M.: A simplified, data-constrained approach to estimate the permafrost carbon–climate
581 feedback, *Philos. Trans. R. Soc. Lond. Ser. A-Math. Phys. Eng. Sci.*, 373, 20140423, doi:
582 10.1098/rsta.2014.0423, 2015.

583 Li, G., Ma, W., Wang, F., Jin, H., Fedorov, A., Chen, D., Wu, G., Cao, Y., Zhou, Y., Mu, Y., Mao, Y.,
584 Zhang, J., Gao, K., Jin, X., He, R., Li, X. and Li, Y.: A newly integrated ground temperature dataset
585 of permafrost along the China–Russia crude oil pipeline route in Northeast China, *Earth Syst. Sci.*
586 *Data*, 14, 5093-5110, doi: 10.5194/essd-14-5093-2022, 2022a.

587 Li, X. and Jin, H.: An integrated dataset of ground hydrothermal regimes and soil nutrients monitored
588 during 2016-2022 in burned areas in Northeast China. National Tibetan Plateau/Third Pole
589 Environment Data Center. doi: 10.11888/Cryos.tpdc.300933, 2024.

590 Li, X., Jin, H., He, R., Wang, H., Sun, L., Luo, D., Huang, Y., Li, Y., Chang, X., Wang, L. and Wei, C.:
591 Impact of wildfire on soil carbon and nitrogen storage and vegetation succession in the Nanweng'he
592 National Natural Wetlands Reserve, Northeast China, *Catena*, 221, 106797, doi:
593 10.1016/j.catena.2022.106797, 2023.

594 Li, X., Jin, H., He, R., Huang, Y., Wang, H., Luo, D., Jin, X., Lu, L., Wang, L., Li, W., Wei, C., Chang,
595 X., Yang, S. and Yu, S.: Effects of forest fires on the permafrost environment in the northern Da
596 Xing'anling (Hinggan) mountains, Northeast China, *Permafr. Periglac. Process.*, 30(3), 163-177,
597 2019.

598 Li, X., Jin, H., Wang, H., Jin, X., Bense, V. F., Marchenko, S. S., He, R., Huang, Y. and Luo, D.: Effects
599 of fire history on thermal regimes of permafrost in the northern Da Xing'anling Mountains, NE
600 China, *Geoderma*, 410, 115670, doi: 10.1016/j.geoderma.2021.115670, 2022b.

601 Li, X., Jin, H., Sun, L., Wang, H., Huang, Y., He, R., Chang, X., Yu, S. and Zang, S.: TTOP-model-based
602 maps of permafrost distribution in Northeast China for 1961–2020, *Permafr. Periglac. Process.*,
603 33(1), 425-435, doi: 10.1002/ppp.2157, 2022c.

604 Li, X., Jin, H., Wang, H., Marchenko, S. S., Shan, W., Luo, D., He, R., Spektor, V., Huang, Y., Li, X. and
605 Jia, N.: Influences of forest fires on the permafrost environment: A review, *Adv. Clim. Change Res.*,
606 12(1), 48-65, 2021.

607 Liang, L., Zhou, Y., Wang, J. and Gao, X.: Changes of the permafrost environment in Great Xian Ridge
608 after disastrous forest fire, Taking Gulian mining area as an example (in Chinese), *J. Glaciol.*
609 *Geocryol.*, 13(1), 17-25, <https://doi.org/10.7522/j.issn.1000-0240.1991.0003>, 1991.

610 Mack, M. C., Bret-Harte, M. S., Hollingsworth, T. N., Jandt, R. R., Schuur, E. A., Shaver, G. R. and
611 Verbyla, D. L.: Carbon loss from an unprecedented Arctic tundra wildfire, *Nature*, 475, 489-492,
612 2011.

613 Mack, M. C., Walker, X. J., Johnstone, J. F., Alexander, H. D., Melvin, A. M., Jean, M. and Miller, S. N.:
614 Carbon loss from boreal forest wildfires offset by increased dominance of deciduous trees, *Science*,
615 372, 280-283, doi: 10.1126/science.abf3903, 2021.

616 Michaelides, R. J., Schaefer, K., Zebker, H. A., Parsekian, A., Liu, L., Chen, J. Y., Natali, S., Ludwig, S.
617 and Schaefer, S. R.: Inference of the impact of wildfire on permafrost and active layer thickness in
618 a discontinuous permafrost region using the remotely sensed active layer thickness (ReSALT)
619 algorithm, *Environ. Res. Lett.*, 14, 035007, //doi: 10.1088/1748-9326/aaf932, 2019.

620 Munkhjargal, M., Yadamsuren, G., Yamkhin, J. and Menzel, L.: The combination of wildfire and
621 changing climate triggers permafrost degradation in the Khentii Mountains, northern Mongolia.
622 *Atmosphere*, 11(2), 155, [https:// doi.org/10.3390/atmos11020155](https://doi.org/10.3390/atmos11020155), 2020.

623 Neff, J. C., Harden, J. W. and Gleixner, G.: Fire effects on soil organic matter content, composition, and
624 nutrients in boreal interior Alaska. *Can. J. For. Res.*, 35(9), 2178-2187, 2005.

625 Nelson, D. W., Sommers, L., Page, A. L., Miller, R. H. and Keeney, D. R., Total carbon, organic carbon,
626 and organic matter. In: Sparks, D. L., Page, A. L., Helmke, P. A. and Loeppert, R. H. eds, *Methods*
627 *of Soil Analysis, Part 3*, Soil Science Society of America. Madison, WI, USA, pp. 539-552, 1982.

628 Nossov, D. R., Jorgenson, M. T., Kielland, K. and Kanevskiy, M. Z.: Edaphic and microclimatic controls
629 over permafrost response to fire in interior Alaska, *Environ. Res. Lett.*, 8, 035013, doi:
630 10.1088/1748-9326/8/3/035013, 2013.

631 O'Donnell, J. A., Harden, J. W., McGuire, A. D., Kanevskiy, M. Z., Jorgenson, M. T. and Xu, X.: The
632 effect of fire and permafrost interactions on soil carbon accumulation in an upland black spruce
633 ecosystem of interior Alaska: Implications for post-thaw carbon loss, *Glob. Change Biol.*, 17(3),
634 1461-1474, 2011a.

635 O'Donnell, J. A., Harden, J. W., McGuire, A. D. and Romanovsky, V. E.: Exploring the sensitivity of soil
636 carbon dynamics to climate change, fire disturbance and permafrost thaw in a black spruce
637 ecosystem, *Biogeosciences*, 8(5), 1367-1382, 2011b.

638 Petrov, M. I., Fedorov, A. N., Konstantinov, P. Y. and Argunov, R. N.: Variability of permafrost and
639 landscape conditions following forest fires in the Central Yakutian Taiga Zone, *Land*, 11, 496, doi:
640 10.3390/land11040496, 2022.

641 Ping, C. L., Michaelson, G. J., Kane, E. S., Packee, E. C., Stiles, C. A., Swanson, D. K. and Zaman, N.
642 D.: Carbon stores and biogeochemical properties of soils under black spruce forest, Alaska, *Soil Sci.*
643 *Soc. Am. J.*, 74, 969-978, doi: 10.2136/sssaj2009.0152, 2010.

644 Ramm, E., Ambus, P. L., Gschwendtner, S., Liu, C., Schloter, M. and Dannenmann, M.: Fire intensity
645 regulates the short-term postfire response of the microbiome in Arctic tundra soil. *Geoderma*, 438,
646 116627, <https://doi.org/10.1016/j.geoderma.2023.116627>, 2023.

647 Rocha, A. V., Loranty, M. M., Higuera, P. E., Mack, M. C., Hu, F., Jones, B. M., Breen, A. L., Rastetter,
648 E. B., Goetz, S. J. and Shaver, G. R.: The footprint of Alaskan tundra fires during the past half-
649 century: implications for surface properties and radiative forcing. *Environ. Res. Lett.*, 7(4), 044039,
650 <https://doi.org/10.1088/1748-9326/7/4/044039>, 2012.

651 Şerban, R.D., Şerban, M., He, R., Jin, H., Li, Y., Li, X., Wang, X. and Li, G.: 46-Year (1973-2019)
652 permafrost landscape changes in the Holo Basin, Northeast China using machine learning and
653 object-based classification, *Remote Sens.*, 13, 1910, doi: 10.3390/rs13101910, 2021.

654 Shur, Y. L. and Jorgenson, M. T.: Patterns of permafrost formation and degradation in relation to climate
655 and ecosystems, *Permafr. Periglac. Process.*, 18(1), 7-19, 2007.

656 Smith, S. L., O'Neill, H. B., Isaksen, K., Noetzli, J. and Romanovsky, V. E.: The changing thermal state
657 of permafrost, *Nat. Rev. Earth Environ.*, 3, 10-23, 2022.

658 Smith, S. L., Riseborough, D. W. and Bonnaventure, P. P.: Eighteen year record of forest fire effects on
659 ground thermal regimes and permafrost in the Central Mackenzie Valley, NWT, Canada, *Permafr.*

660 Periglac. Process., 26(4), 289-303, 2015.

661 Soil Survey Staff.: Keys to Soil Taxonomy, 12th Edition. Natural Resources Conservation Service,
662 United States Department of Agriculture, Washington D.C., 2014.

663 Sun, L., Zhao, J. and Hu, H.: Effect of moderate fire disturbance on soil physical and chemical properties
664 of *Betula platyphylla-Larix gmelinii* mixed forest (in Chinese), *Sci. Silvae Sinicae*, 47(2), 103-110,
665 2011.

666 Taş, N., Prestat, E., McFarland, J. W., Wickland, K. P., Knight, R., Berhe, A. A., Jorgenson, T., Waldrop,
667 M. P. and Jansson, J. K.: Impact of fire on active layer and permafrost microbial communities and
668 metagenomes in an upland Alaskan boreal forest. *ISME J.*, 8(9), 1904-1919, 2014.

669 Turetsky, M. R., Abbott, B. W., Jones, M. C., Anthony, K. W., Olefeldt, D., Schuur, E. A. G., Koven, C.,
670 McGuire, A. D., Grosse, G., Kuhry, P., Hugelius, G., Lawrence, D. M., Gibson, C. and Sannel, A.
671 B. K.: Permafrost collapse is accelerating carbon release, *Nature*, 569, 32-34, 2019.

672 Viereck, L.A., Werdin-Pfisterer, N.R., Adams, P.C. and Yoshikawa, K.: Effect of wildfire and fireline
673 construction on the annual depth of thaw in a black spruce permafrost forest in interior alaska: a 36-
674 year record of recovery. In Kane DL and Hinkel KM eds, *Proceedings of the Ninth International
675 Conference on Permafrost*, Fairbanks, Alaska, USA, June 29 to 3 July, Vol. 2, pp. 1845-1850, 2008.

676 Wang, H., Jin, H., Che, T., Li, X., Dai, L., Qi, Y., Huang, C., He, R., Zhang, J., Yang, R., Luo, D. and Jin,
677 X.: Influences of snow cover on the thermal regimes of Xing'an permafrost in Northeast China in
678 1960s–2010s, *Permafrost Periglac. Process.*, 35(2), 188-201, doi: 10.1002/ppp.2223, 2024.

679 Westerling, A. L., Hidalgo, H. G., Cayan, D. R. and Swetnam, T. W.: Warming and earlier spring increase
680 Western U.S. forest wildfire activity, *Science*, 313, 940-943, doi: 10.1126/science.1128834, 2006.

681 Xu, W., Elberling, B. and Ambus, P. L.: Long-term summer warming reduces post-fire carbon dioxide
682 losses in an arctic heath tundra, *Agric. For. Meteorol.*, 344, 109823, doi:
683 10.1016/j.agrformet.2023.109823, 2024

684 Yoshikawa, K., Bolton, W. R., Romanovsky, V. E., Fukuda, M. and Hinzman, L. D.: Impacts of wildfire
685 on the permafrost in the boreal forests of Interior Alaska, *J. Geophys. Res.*, 108, 8148, doi:
686 10.1029/2001JD000438, 2003.

687 Zhao, L., Zou, D., Hu, G., Wu, T., Du, E., Liu, G., Xiao, Y., Li, R., Pang, Q., Qiao, Y., Wu, X., Sun, Z.,
688 Xing, Z., Sheng, Y., Zhao, Y., Shi, J., Xie, C., Wang, L., Wang, C. and Cheng, G.: A synthesis dataset
689 of permafrost thermal state for the Qinghai–Tibet (Xizang) Plateau, China, *Earth Syst. Sci. Data*,
690 13, 4207-4218, 2021.

691 Zhou, Y., Liang, L. and Gu, Z.: Effects of forest fire on hydro-thermal regime of frozen ground, the
692 northern part of the Da Hinggan Ling (in Chinese), *J. Glaciol. Geocryol.*, 15, 17-26, 1993.